DNS of a Mach 4 Boundary Layer with Chemical Reactions

M. Pino Martín*
Graham V. Candler†
Aerospace Engineering and Mechanics
University of Minnesota, Minneapolis, MN 55455

Abstract

A direct numerical simulation (DNS) database is used to develop a greater understanding of the turbulence-chemistry interaction in hypersonic boundary layers. It is found that exothermic reactions increase the turbulent dissipation near the wall, the large turbulent structure inclination angles, and the magnitude of turbulent fluctuations. The opposite is found for endothermic reactions in the boundary layer.

Introduction

The boundary layer on future air-breathing hypersonic cruise vehicles will be turbulent and chemically reacting. To aid the design of such vehicles, a greater understanding of turbulent hypersonic flows is needed. Thus far, our understanding of the interaction between turbulent motion and chemical reactions in hypersonic flows is limited. With the very high energies present in these flows, the temperature fluctuations are very large. The reaction rate depends exponentially on temperature, and temperature fluctuations result in large increases in the reaction rates. Also, the chemical source term can either damp or amplify turbulent fluctuations. Recently, Johnson *et al.*[1] have also shown that hypersonic boundary layers tend to be stabilized by endothermic reactions and destabilized by exothermic reactions.

In our previous work,[2,3] we used DNS to perform a fundamental study of isotropic turbulence interacting with finite-rate chemical reactions at conditions typical of a hypersonic boundary layer. We found that the turbulent motion is fed from the energy provided by the exothermic reactions, while the reaction rate is increased by the turbulent temperature fluctuations. This is a feedback process that takes place through the pressure-strain term in the Reynolds stress equation. The feedback is negative for endothermic reactions, resulting in a reduction in the turbulent motion.

To generalize the findings from the isotropic simulations, we use DNS to build a database of turbulent boundary layers at hypersonic conditions. These simulations are very difficult to obtain, since there is no previous DNS at high Reynolds and Mach numbers.

In the reminder of the paper, we introduce the flow parameters and discuss the numerical method. We then discuss our procedure to initialize the turbulent compressible field and asses the validity of the resulting turbulent boundary layers. We present the results and analyze the turbulent-chemistry interaction. Finally, we summarize our findings.

Flow Parameters

The boundary layer edge conditions chosen are $Re_\theta = 7000$, $M_\infty = 4.0$, $T_\infty = 5000$ K, and $\rho_\infty = 0.5$ kg/m^3. These conditions represent the boundary layer on a 26° wedge at a Mach number of 20 and 20 km altitude and are illustrated in Fig. 1. In this case, the boundary layer temperature is high enough to induce chemical reactions. We use a single model reaction, $\mathrm{S1} + \mathrm{M} \rightleftharpoons \mathrm{S2} + \mathrm{M}$, where species S1 and S2 have the same molecular weight and number of degrees of freedom. The reaction rates correspond to either nitrogen or oxygen dissociation, which are the most common reactions in a hypersonic boundary layer. To obtain different chemical conditions, simulations with different wall temperatures are considered, namely adiabatic and 5000K. Lower wall temperature simulations are beyond the capability of the 256-processor T3E used in this work.

To assess the turbulence-chemistry interaction, we choose the reaction rate that will show the physics more clearly for the different wall conditions. The chemical reactions are turned on after the boundary layer simulation reaches a stationary state based on obtaining constant distributions of the turbulent kine-

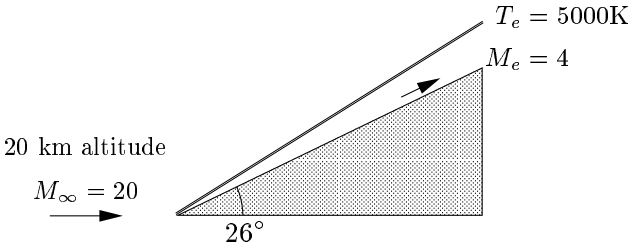

FIGURE 1. Flow conditions for the direct numerical simulation of boundary layers.

* Postdoctoral Fellow, Member AIAA (pino@aem.umn.edu)
† Professor, Senior Member AIAA (candler@aem.umn.edu)

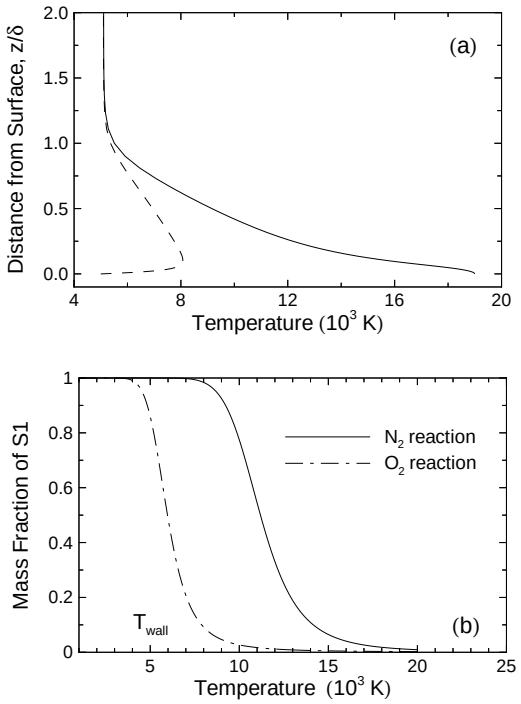

FIGURE 2. Flow parameters for the adiabatic and isothermal boundary layer simulations. (a) Temperature; and (b) temperature dependence of species S1 mass fraction at equilibrium.

etic energy and temperature fluctuations across the boundary layer. The species mass fractions are initialized to their equilibrium values at the mean temperature and density at each plane parallel to the wall. Although the chemical composition in typical hypersonic boundary layers is not in equilibrium, this initialization serves to isolate the effect of turbulent fluctuations in the turbulence-chemistry interaction.

It is illustrative to consider the mean temperature profiles and the equilibrium composition for the reactions chosen. Figure 2a plots the mean temperature profiles. For the adiabatic case, the temperature increases from the boundary layer edge to the wall and the reactions are endothermic. For the isothermal wall simulation, the maximum temperature occurs at some distance from the wall, where there is significant shear heating and the wall cooling is not important. In this region, molecules dissociate and the reaction products diffuse toward the surface where they recombine due to the cold wall. Thus, in the isothermal simulation there is a region of exothermic reactions near the wall.

Figure 2b plots the equilibrium diatomic mass fraction versus temperature for the nitrogen and oxygen dissociation reactions. The minimum temperature for the boundary layer simulations is 5000 K. At this temperature, Fig. 2b indicates that $C_{\mathrm{O}_2} = 0.82$ and $C_{\mathrm{N}_2} = 1$. For the adiabatic simulation, the maximum temperature is 19,000 K and C_{O_2} or C_{N_2} are nearly 0. Thus, for the adiabatic simulations, choosing either nitrogen or oxygen dissociation gives the entire range of species mass fractions within the boundary layer. We chose nitrogen dissociation since the heat of formation for this reaction is larger than for the oxygen reaction, making the effect of the heat removal in the formation of S2 species more apparent.

In the isothermal case, choosing a nitrogen dissociation reaction would give very low levels of dissociation. Thus, the effect of turbulent temperature fluctuations on the equilibrium chemical composition would be difficult to observe. However, oxygen dissociation gives a range of C_{O_2} from roughly 0.1 to 0.9 with a lower activation energy. Therefore, to observe the turbulence-chemistry interaction more clearly in the isothermal case, we model the oxygen dissociation reaction.

Numerical Method

The numerical method combines a weighted essentially non-oscillatory (WENO) scheme for the inviscid fluxes with an implicit time advancement technique. The third-order accurate, high-bandwidth, WENO scheme was designed for low dissipation[4] and provides shock-capturing, which is necessary at the Mach numbers considered. The time advancement technique is based on the DPLU relaxation method of Candler *et al.*[5] and was extended to second-order accuracy by Olejniczak & Candler.[6] The derivatives required for the viscous terms are evaluated using 4th-order central differences.

Figure 3 plots the mean velocity profile for a non-reacting turbulent boundary layer at $Re_\theta = 930$, $M = 0.3$, $T_{\mathrm{wall}} = T_\infty = 300$ K, and $\rho_\infty = 1$ kg/m^3. The velocity profile is in good agreement with the theoret-

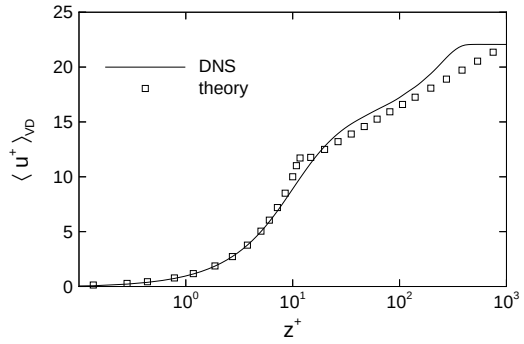

FIGURE 3. Mean velocity profile scaled on inner variables, and compared to the theoretical $u^+ = z^+$, and Van-Driest empirical $u^+ = 2.44 \log z^+ + 5.2$ scaling laws for a boundary layer at $M = 0.3$, $Re_\theta = 930$.

ical viscous sublayer and logarithmic region. The implementation of the numerical scheme has been successfully validated[7] by comparing this simulation to experimental data.

DNS Initial Conditions

The initialization of turbulence is the art of making an educated guess. In our simulations, the mean velocity, density, and temperature profiles, and the inner parameters

$$u_\tau = \sqrt{\frac{\mu_w \left(\frac{\partial u}{\partial z}\right)_w}{\rho_w}}, \qquad z_\tau = \frac{\mu_w}{\rho_w u_\tau},$$

at the desired Mach number are obtained from a $k-\epsilon$ Reynolds-averaged Navier-Stokes simulation.[8] The fluctuating velocity field is obtained by normalizing the Mach 0.3 velocity fluctuations[7] by the ratio of the inner parameters at the high Mach number to that at M =0.3. In this way, the initial fluctuating field is scaled in proportion to the Mach number. The turbulent field is mapped onto a computational domain that is also normalized in wall units. Thus, the initial turbulence structures and energy spectra resemble those of a realistic turbulent boundary layer. Also, using this initialization method we avoid introducing spurious acoustic waves into the computational domain. The initial fluctuations in the thermodynamic variables are estimated using the strong Reynolds analogy.[9]

The computational domain size and grid resolution required for the simulations has been carefully determined. A DNS must resolve all turbulent scales from the large energy containing eddies down to the dissipative scales. Dissipation takes place in the range $0.1 < k\eta < 1$ where k is the wavenumber and η is the Kolmogorov length scale. Thus, a DNS must resolve scales of order η. Furthermore, the size of the domain must be large enough to enclose a good statistical sample of the large structures in the field. The number of grid points required is proportional to $L/\eta \sim Re^{3/4}$, where L is the domain size, and Re is the Reynolds number based on the integral scale of the flow. For a three-dimensional DNS the number of grid points is proportional to Re.[9/4] This estimate serves as an upper-bound approximation to the number of grid points required.[10] In practice, an optimal number of grid points may be determined based on previous DNS (not available for the conditions chosen), and by monitoring the energy spectra and the two-point correlations in the turbulent flow of interest. A well resolved energy spectrum shows at least two decades of turbulence decay, indicating that the dissipation range is well resolved. Also, the two-point correlations must vanish in the middle of the domain, indicating that the turbulence statistical sample is large enough.

T_w	δ^+	Δx^+	Δy^+	L_x/δ	L_y/δ	L_z/δ
adiabatic	700	15	11	8	2	14
5000 K	2400	22	16	3.5	0.8	13

TABLE 1. Grid resolution and domain size for the $M = 4$, $Re_\theta = 7000$, and $T_\infty = 5000$ K boundary layer simulations.

To better illustrate the resolution and the domain size requirements, let us consider the flow topology given by our DNS. When using iso-surfaces of the vorticity magnitude to visualize the three-dimensional flow topology, the plots look cloudy making it difficult to identify the structures. Also, the second invariant of the velocity gradient tensor,[11] Φ, does not have the proper physical meaning to identify the turbulent structures in a compressible flow. Thus, it is not clear whether Φ should be used to visualize the flow topology in this study. Instead, we chose to identify the turbulence structures using the swirl strength, λ_{ci}, as defined by Zhou *et al.*[12] Figure 4 plots iso-surfaces of λ_{ci}^2 to identify the large structures in the simulations, i.e. in a domain normalized in δ units. Note that the x, y, and z coordinates correspond to the streamwise, spanwise, and wall-normal directions, respectively. Comparing Figures 4a and 4b, we observe that the structures are larger for the adiabatic simulation. Thus, to enclose a good statistical sample of the large structures, the computational domain must be larger for the adiabatic case than for the isothermal case.

Figure 5 plots iso-surfaces of λ_{ci} in a domain normalized in wall units. We observe that the structures are larger for the isothermal simulation, when plotted in this fashion. Thus, to resolve the streaks that form in the viscous sublayer, we can use a larger grid resolution in wall units.

The conclusions drawn from Figures 4 and 5 can also be inferred (prior to performing the DNS) from the ratio of the small to large scales for each simulation. Consider the grid resolution and domain size for the simulations given in Table 1. The two simulations have the same Re_θ, and δ is nearly the same for all cases. In contrast, z_τ decreases with decreasing wall temperature. We observe that as the wall temperature decreases, the ratio of the large to small scales, $\delta^+ = \delta/z_\tau$, increases. Thus, the number of discrete scales of motion increases as well, as seen in

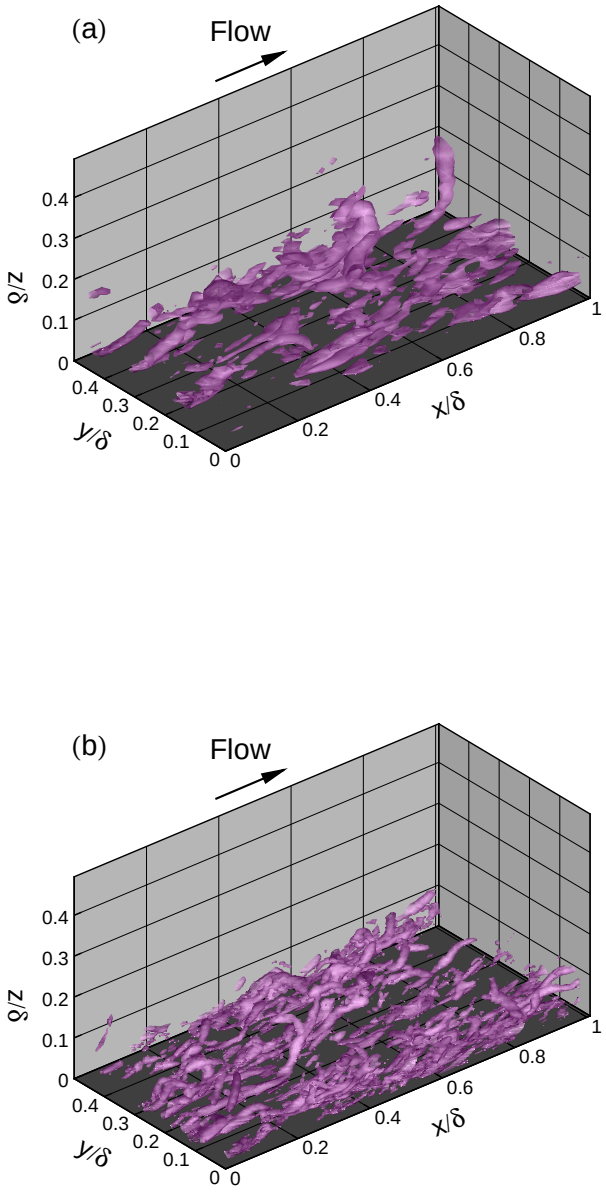

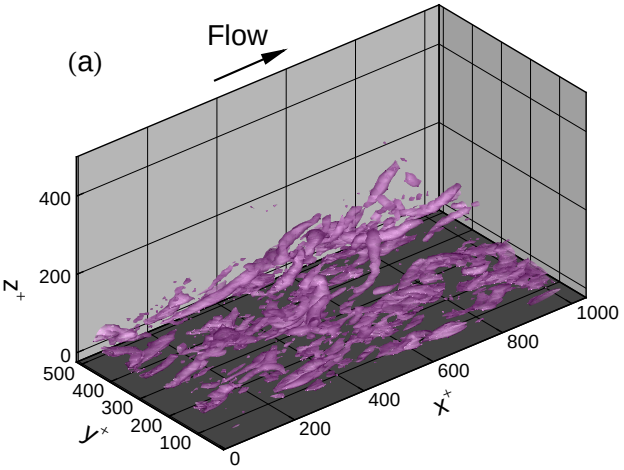

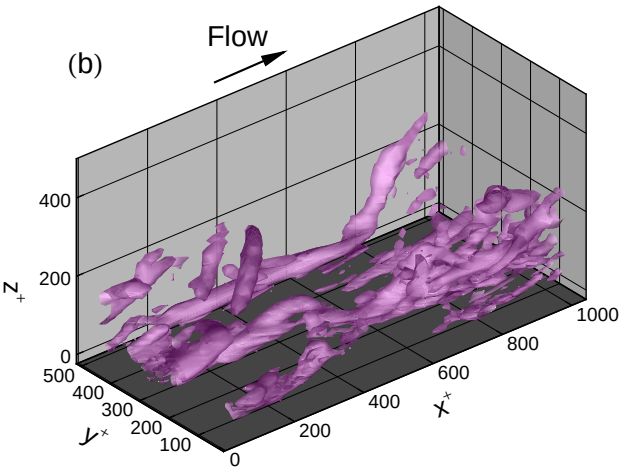

FIGURE 4. Flow structure visualized using iso-surfaces of λ_{ci}^2 with 1% of the maximum value for the (a) adiabatic and (b) isothermal boundary layer simulations. Coordinates are given in δ units.

FIGURE 5. Flow structure visualized using iso-surfaces of λ_{ci}^2 with 1% of the maximum value for the (a) adiabatic and (b) isothermal boundary layer simulations. Coordinates are given in z_τ units.

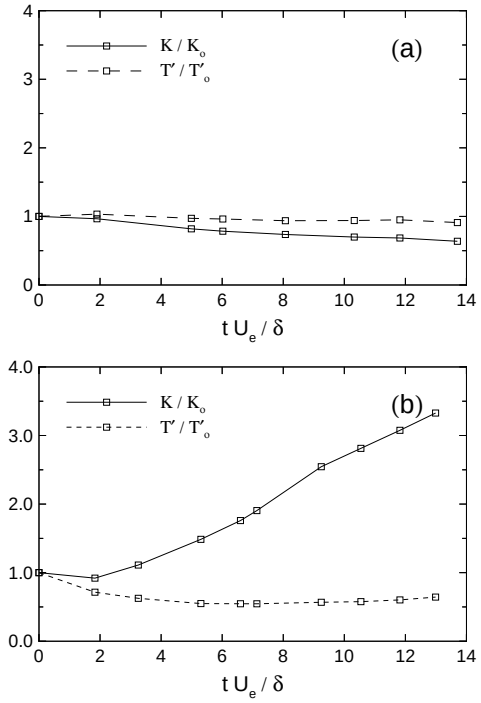

FIGURE 6. Time history of the bulk turbulent kinetic energy, $K/K_\circ$, and root-mean-square temperature fluctuations, $T'/T'_\circ$, for the (a) adiabatic; and (b) isothermal boundary layer simulations at $M = 4$ and $Re_\theta = 7000$ prior to starting the chemical reactions.

Fig. 4. In turn, the isothermal simulation requires a larger number of grid points. It is found that for the adiabatic simulation, the lengths of 8δ and 2δ in the streamwise and spanwise directions, respectively, are adequate. For the isothermal simulation, 3.5δ, and 0.8δ are sufficient. In the wall-normal direction, the height of the domain is determined so that acoustic disturbances originating at the upper boundary do not interact with the boundary layer on the lower wall. The grid is stretched in the wall-normal direction. For both cases, the grid-stretching factor is 1.069, the first point away from the wall is located at $z^+ = 0.13$, and there are 21 grid points below $z^+ = 10$. The number of grid points to achieve the required resolution are $(384 \times 128 \times 128)$ and $(384 \times 128 \times 150)$ for the adiabatic and isothermal simulations, respectively. Note that although the resolution in wall units is coarser for the isothermal simulation, the resolution in δ units is nearly twice as large as for the adiabatic case.

Throughout the simulations, the above resolution and domain size conditions satisfy the required decay in the energy spectra and the vanishing of the two-point correlations in the middle of the computational domain, indicating well resolved DNS.

We use supersonic boundary conditions in the free stream and periodic boundary conditions in the streamwise and spanwise directions. Thus, the boundary layer is temporally developing. Low-speed simulations with periodic boundary conditions may not be valid, since the amount of kinetic energy in the free stream may not be sufficient to maintain the turbulence levels in the boundary layer. However, this is not an issue in the present simulations, since the kinetic energy in the free stream is substantial.

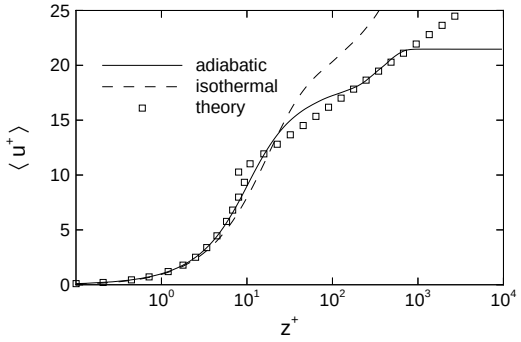

FIGURE 7. Mean velocity profile scaled on inner variables, and compared to the theoretical $u^+ = z^+$, and Van-Driest empirical $u^+ = 2.44 \log z^+ + 5.2$ scaling laws for the adiabatic and isothermal simulations at $M = 4$ and $Re_\theta = 7000$ prior to starting the chemical reactions.

Flow Assessments

We look for a steady-state turbulence prior to initiating the chemical reactions. Ideally, this state should be based on a steady-state distribution of the turbulent kinetic energy and temperature fluctuations across the boundary layer. Figure 6 plots the time history of the bulk turbulent kinetic energy and the root-mean-square temperature fluctuations for the simulations prior to turning on the reactions. For the adiabatic simulation, Fig. 6a, the turbulent kinetic energy reaches an equilibrium state near $t = 10\tau_\Lambda = 10\delta/U_e$, where the solid line begins to flatten. The distribution of temperature fluctuations is nearly at equilibrium at $5\tau_\Lambda$. Thus, for this simulation, we turn on the chemistry at $10\tau_\Lambda$.

The isothermal simulation presents some difficulties, as seen in Fig. 6b. The turbulent kinetic energy increases monotonically in time. It is clear that this simulation has not reached equilibrium. To date, we have not found the reason for this result. However, the magnitude of the temperature fluctuations remains nearly steady after $7\tau_\Lambda$. For this simulation, we choose to turn on the reactions at $13\tau_\Lambda$.

Figure 7 plots the mean velocity scaled on the inner variables for the adiabatic and isothermal simula-

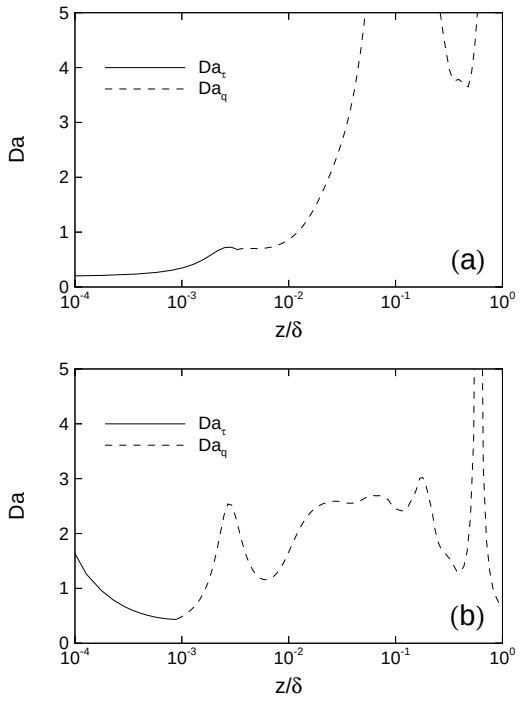

FIGURE 8. Damköhler numbers , $Da_\tau = \tau_c u_\tau/\delta$ in the buffer region and $Da_q = \tau_c q/\delta$ elsewhere, for the for the (a) adiabatic; and (b) isothermal simulations.

tions at 10 and $13\tau_\Lambda$, respectively. The velocity profile for the adiabatic simulation is in good agreement with the theoretical predictions. However, the data for the isothermal simulation fails to match the empirical laws.

Although, the isothermal simulation is not in equilibrium to date, the typical flow structures of wall turbulence can still be found. Therefore, although care must be taken when considering the isothermal results quantitatively, the turbulence-chemistry interaction may still be assessed. After starting the reactions, we reset the time to zero.

An issue to consider when performing DNS of temporally developing boundary layers is the growth of the displacement thickness, δ^*. δ^* represents the distance by which the streamlines in the boundary layer edge are shifted due to the temporal development of the boundary layer. Significant growth of δ^* may affect the important flow statistics. In the following, we assess the growth of δ^* during the data-collection time for the reacting simulations.

Let us define the relevant characteristic turbulent time scales across the boundary layer. We assume that the low-speed, streaky structures that are formed in the viscous sublayer evolve at a τ_τ time scale, where $\tau_\tau = \delta/u_\tau$. Similarly, we define a different turbulent time scale as $\tau_q = \delta/q$, where $q = \langle u_i' u_i' \rangle$ that may represent the temporal evolution of the larger structures that form in the buffer and logarithmic regions. The chemical time scale can be defined[3] as $\tau_c = \langle\rho\rangle/|\ \omega_s \log(K_{\rm eq})\ |$, where ω_s is the chemical source term of species s, namely

$$w_{\rm S1} = \left(-M_{\rm S1} k_f \frac{\rho_{\rm S1}}{M_{\rm S1}} + M_{\rm S1} k_b \frac{\rho_{\rm S2}}{M_{\rm S2}}\right) \sum_s \frac{\rho_s}{M_s},$$

and $w_{\rm S2} = -w_{\rm S1}$, with M_s and ρ_s as the molecular weight and density of species s, respectively; and k_f and k_b are the forward and backward reaction rates. These are written as

$$k_f = C_f\, T^\eta\, e^{-\theta/T},$$
$$k_b = \frac{k_f}{K_{eq}},$$

where K_{eq} is the temperature-dependent equilibrium constant. Thus, we can define two Damköhler numbers,

$$Da_\tau = \frac{\tau_\tau}{\tau_c},$$
$$Da_q = \frac{\tau_q}{\tau_c},$$

which represent the non-dimensional reaction rates characteristic of the different regions in the boundary layer.

Figure 8a plots Da_τ and Da_q for the adiabatic simulation. We observe that the chemistry is very slow relative to the turbulence evolution at the wall. When τ_c and the turbulent time scale are not of the same order of magnitude, the chemistry and turbulence evolve uncoupled from each other.[3] Thus, in the viscous sublayer, the chemistry does not affect the turbulence significantly so that the turbulence-chemistry interaction does not evolve at a τ_τ time scale. However, Da_q is $\mathcal{O}(1)$ in a portion of the boundary layer. Thus, to study the turbulence chemistry interaction at these conditions we should gather statistics over at least one τ_q period of time. The growth of δ^* in one τ_q is 4%, which is negligible. Thus, periodic boundary conditions are suitable for the adiabatic simulation.

For the isothermal simulation, Fig. 8b shows that Da_τ is $\mathcal{O}(1)$ in the viscous sublayer. Thus, we expect the turbulence chemistry interaction to be important in a τ_τ time scale. For the isothermal simulation, δ^* varies less than 2% in $0.5\tau_\tau$. Thus, periodic boundary conditions are also suitable for the adiabatic simulation.

Figure 9 plots the ratio of the average mass fraction of species S1 to its equilibrium value at the conditions across the boundary layer, giving a measure of the chemical non-equilibrium. For the adiabatic simulation, the time is $t = \tau_\Lambda = 0.5\tau_q$ and we observe that

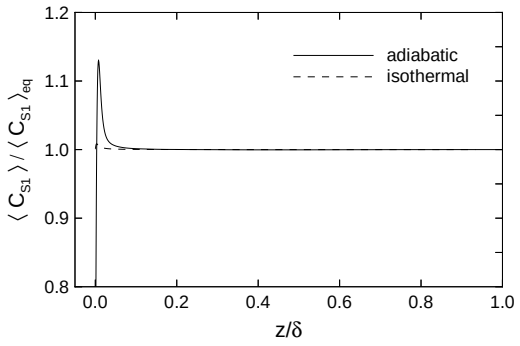

FIGURE 9. Average mass fraction normalized by the average equilibrium mass-fraction value, $\langle C_{\rm S1}\rangle/\langle C_{\rm S1}\rangle_{\rm eq}$, for the adiabatic and isothermal simulations at $t/\tau_\Lambda = 1$ and 8, respectively.

the boundary layer has reached chemical equilibrium everywhere except at the wall. For the isothermal simulation, the time is $t = 8\tau_\Lambda = 0.5\tau_\tau$ and the boundary layer has reached chemical equilibrium as well. Thus, our time scale estimates are valid.

Turbulence-Chemistry Interaction

Let us first consider the results for the adiabatic simulation. Note that the reaction is primarily endothermic for the conditions chosen as species S1 is destroyed to form S2. Figure 10 plots mass-fraction contours of species S1 on spanwise planes of data at the initial and final times. The initial condition is chemical equilibrium at the plane-average temperature. At $4\tau_\Lambda$, the fluctuations in $C_{\rm S1}$ are apparent. However, it is difficult to determine whether the changes in $C_{\rm S1}$ are due to destruction of species or to turbulent mixing. Figure 11 plots temperature contours for the same data set. We observe a reduction in the wall temperature, which corresponds to an 1800 K reduction in the average wall temperature. We also observe that the temperature fluctuations are reduced, and the strength of the bursting events associated with the larger structures in the boundary layer, is reduced as well. Note also by comparing Figures 10 and 11 that regions of low $C_{\rm S1}$ correspond to high temperature regions, which indicates S2 formation due to the turbulent temperature fluctuations. This maybe seen more quantitatively in Fig. 12, which plots $\langle T\rangle$ and $T'_{\rm RMS}$ in the boundary layer. We observe significant reduction in the wall temperature and in the magnitude of the temperature fluctuations across the boundary layer. This indicates that the chemical reactions occur at the expense of the turbulent temperature fluctuations.

Now consider how the turbulence-chemistry interaction affects the vorticity. Figure 13 plots spanwise vorticity contours in the streamwise direction for the same data as above. Comparing the initial and final fields, we observe that the range of turbulent scales is reduced. The strength of the large structures is also reduced. Furthermore, we observe a reduction in the angle of inclination of the turbulent structures when endothermic reactions occur.

Let us now consider the isothermal simulation, where the reactions are exothermic near the wall as species S1 is formed. Figure 14 plots mass fraction contours of species S1 on spanwise planes of data. At the final time we observe an increase of species S1 near the wall, indicating that the exothermic recombination reaction occurs at the wall. Also, near $z/\delta = 0.3$ the amount of S1 increases, however as we will demonstrate later, this is not due to production of species S1 but rather to turbulent mixing that redistributes the chemical species. It is interesting to consider the temperature contours for the same planes of data. Figure 15 shows a reduction of the temperature across the boundary layer, including the near wall region, where exothermic reactions occur. In contrast to the previous simulation, the gradients of temperature are steeper after the reactions occur, indicating an increase in the turbulent temperature fluctuations.

Figure 16 plots the streamwise component of vorticity for the same spanwise planes of data. Comparing the initial and final fields, we see that the larger turbulent structures extend farther from the wall reaching roughly $z/\delta = 0.4$, where initially they extended to about $z/\delta = 0.2$. Furthermore, the scales in the near-wall region are smaller and flatter after the exothermic reactions occur. Figure 17 plots the spanwise vorticity along the streamwise direction for the same data. We find that the inclination of the structures near the wall is increased by the exothermic reactions.

Figure 18 plots the mean temperature and S1 mass-fraction profiles. We observe that the peak in the mean temperature decreases. This is because although exothermic reactions occur at the wall, the energy is transferred to the turbulent modes, not to the mean internal energy. Also, we see that the mass fraction of S1 increases, which is not due to the formation of S1, but rather to the turbulent mixing enhancement by the exothermic reactions that occur at the wall. The physical mechanisms that generate this result can be explained as follows. Near the wall, S1 is produced due to the colder temperature, and energy is released. In turn, the gas expands upwards and downward. The downwards expansion compresses the near wall streaky structures, which become flatter and break up into smaller scales due to the enhanced compressible dissipation. In contrast, the upwards expansion lifts the

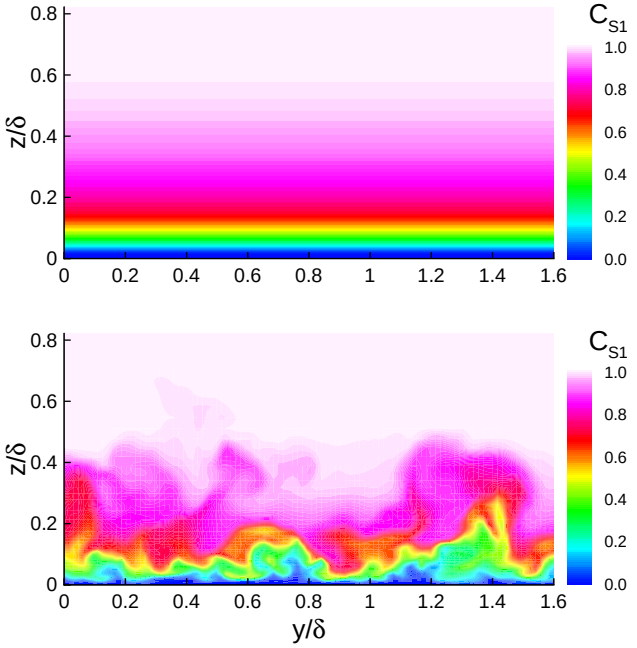

FIGURE 10. S1 mass-fraction contours in the spanwise direction for the adiabatic simulation. (a) $t/\tau_\Lambda = 0$; (b) $t/\tau_\Lambda = 4$.

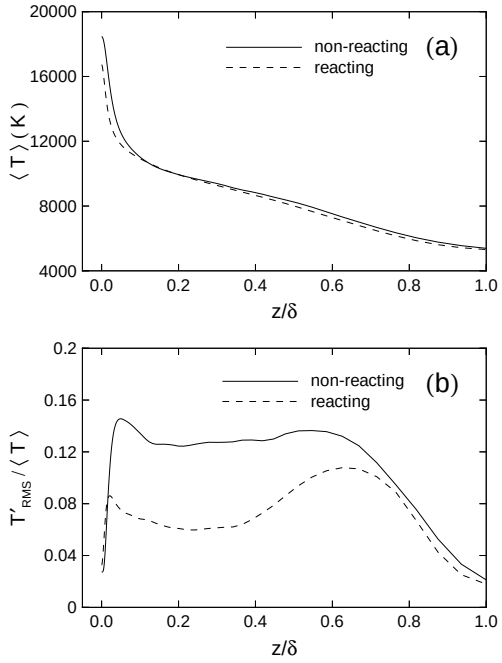

FIGURE 12. (a) Mean temperature and (b) normalized magnitude of the temperature fluctuations for the adiabatic simulation.

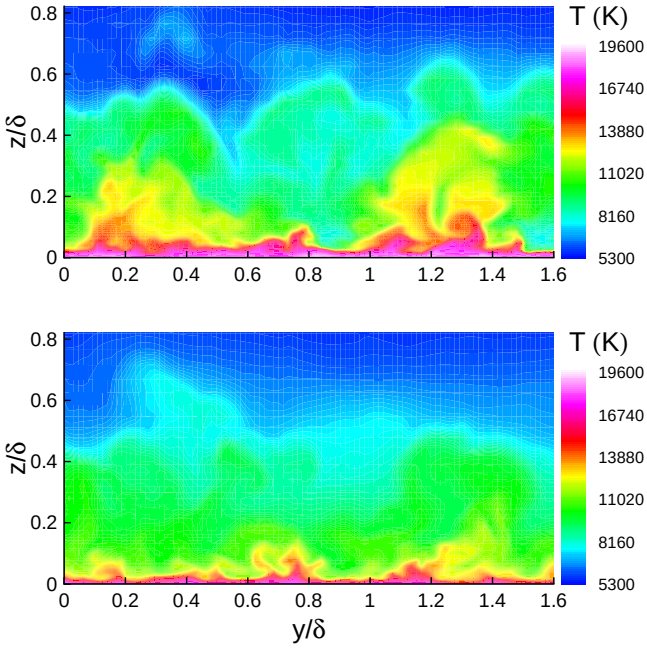

FIGURE 11. Temperature contours in the spanwise direction for the adiabatic simulation. (a) $t/\tau_\Lambda = 0$; (b) $t/\tau_\Lambda = 4$.

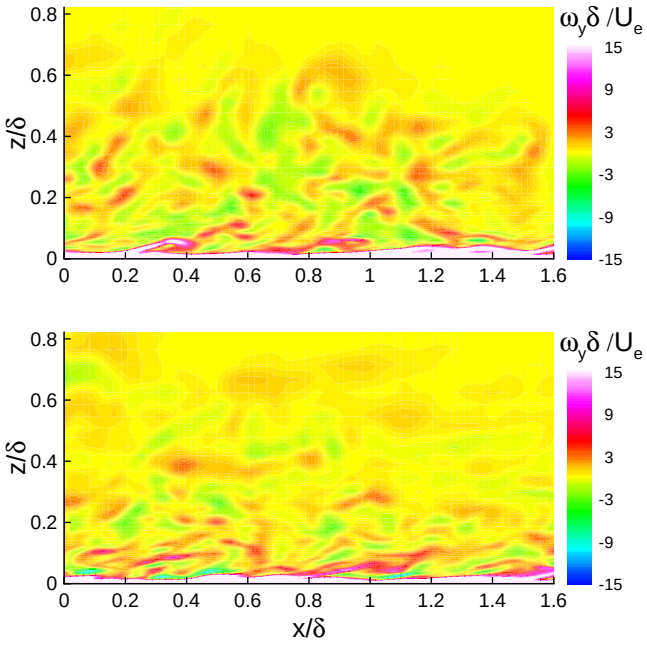

FIGURE 13. Spanwise vorticity contours in the streamwise direction for the adiabatic simulation. (a) $t/\tau_\Lambda = 0$; (b) $t/\tau_\Lambda = 4$.

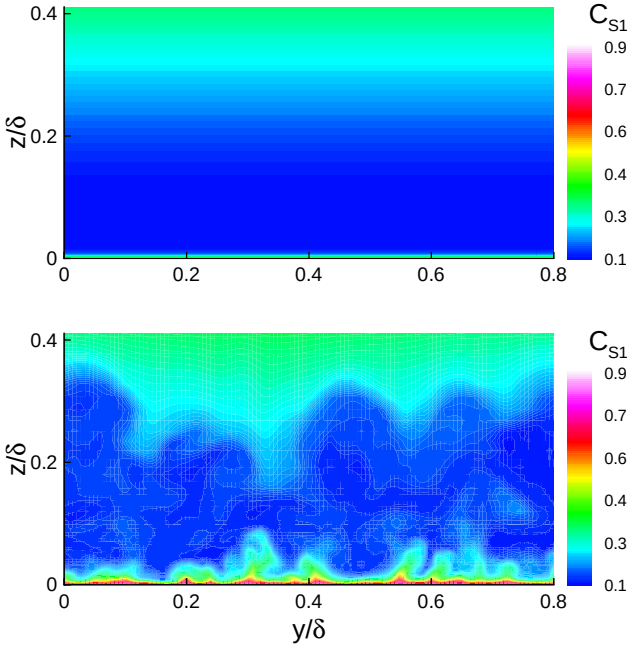

FIGURE 14. S1 mass-fraction contours in the spanwise direction for the isothermal simulation. (a) $t/\tau_\Lambda = 0$; (b) $t/\tau_\Lambda = 8$.

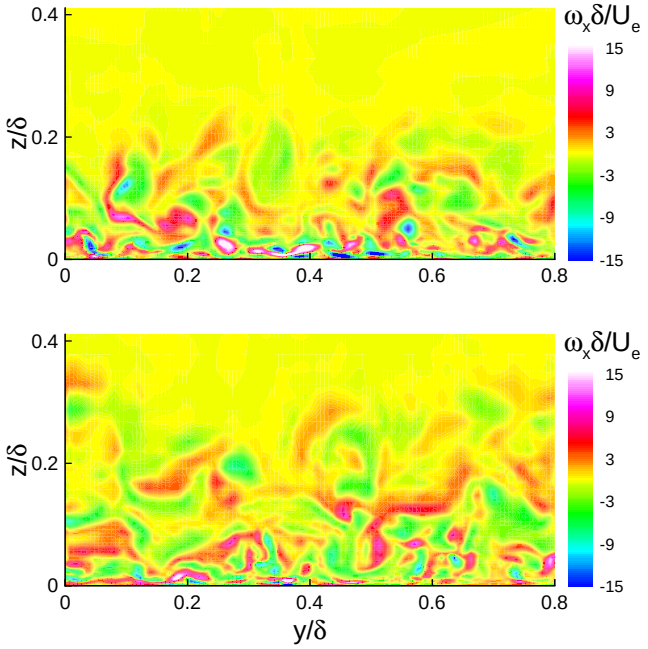

FIGURE 16. Streamwise vorticity contours in the spanwise direction for the isothermal simulation. (a) $t/\tau_\Lambda = 0$; (b) $t/\tau_\Lambda = 8$.

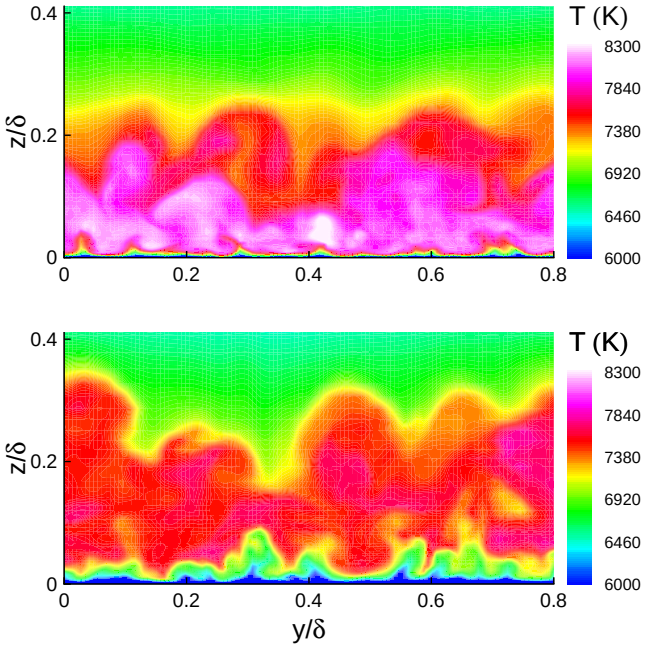

FIGURE 15. Temperature contours in the spanwise direction for the isothermal simulation. (a) $t/\tau_\Lambda = 0$; (b) $t/\tau_\Lambda = 8$.

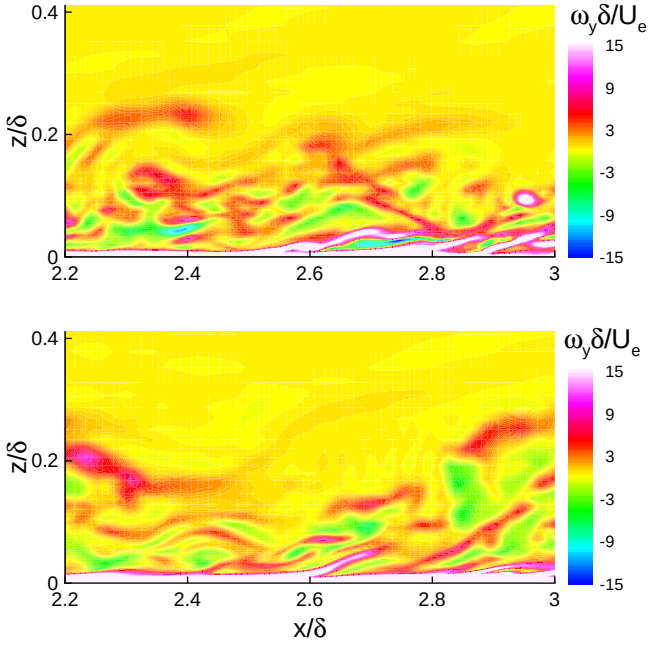

FIGURE 17. Spanwise vorticity contours in the streamwise direction for the isothermal simulation. (a) $t/\tau_\Lambda = 0$; (b) $t/\tau_\Lambda = 8$.

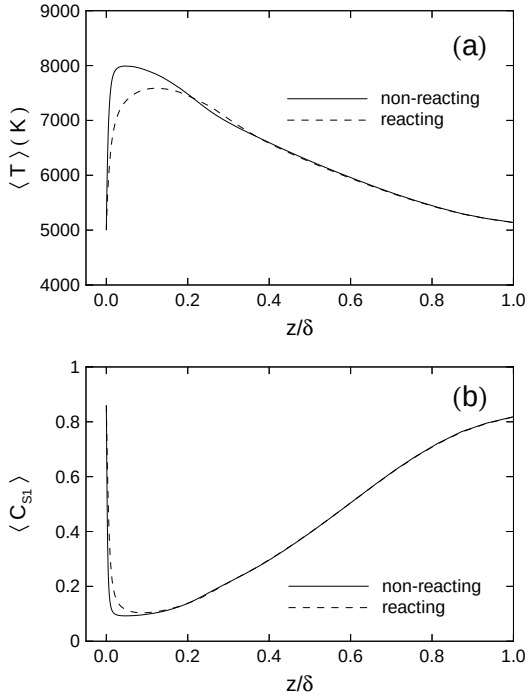

FIGURE 18. Mean (a) temperature and (b) species S1 mass fraction for the isothermal simulation.

large ("hairpin") turbulent structures, which are also stretched by the mean convection. The net result is enhanced turbulence levels and a larger turbulent mixing region in the boundary layer. Evidence of these mechanisms has also been observed in the vorticity and Reynolds stress budgets. Although exothermic reactions occur, we observe a reduction in the mean temperature. This effect is due to the larger turbulent mixing, which reduces the peak in the mean temperature profile and redistributes the chemical species across the boundary layer. Since finite-rate reactions are temperature limited, the redistribution of species does not activate the chemical process. Thus, the increased values of S1 are not due to the chemical reactions.

Figure 19 plots the magnitude of the temperature fluctuations across the boundary layer for the isothermal simulation. Consistent with the argument made above, the magnitude of the temperature fluctuations increases near the wall due to the exothermic reactions. Away from the wall the mixing mechanisms reduce the secondary peak in the temperature fluctuation profile.

Finally, Fig. 20a plots the time history of the bulk turbulent kinetic energy and the root-mean-squared of the temperature fluctuations for the adiabatic simulation. The endothermic reactions damp the temperature fluctuations. Note that the boundary layer reaches chemical equilibrium in one τ_Λ. Thus, the temperature fluctuations are damped in one τ_Λ. At later times, the temperature fluctuations increase slowly as the turbulent kinetic energy dissipates. The bulk turbulent kinetic energy is not affected by the endothermic reactions. Similarly, Fig. 20b plots the same variables for the isothermal simulation. We observe that the exothermic reactions increase the turbulent temperature fluctuations. The bulk turbulent kinetic energy increases as well. These results are consistent with those previously found in isotropic turbulence at conditions typical of hypersonic boundary layers.[2]

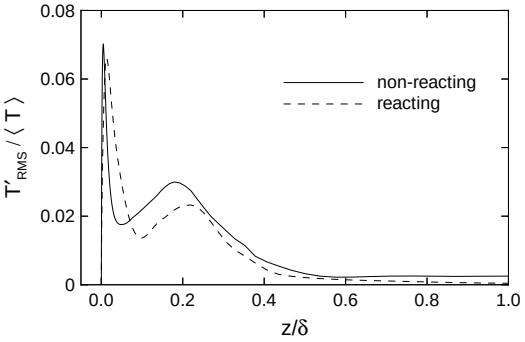

FIGURE 19. Normalized magnitude of the temperature fluctuations for the isothermal simulation.

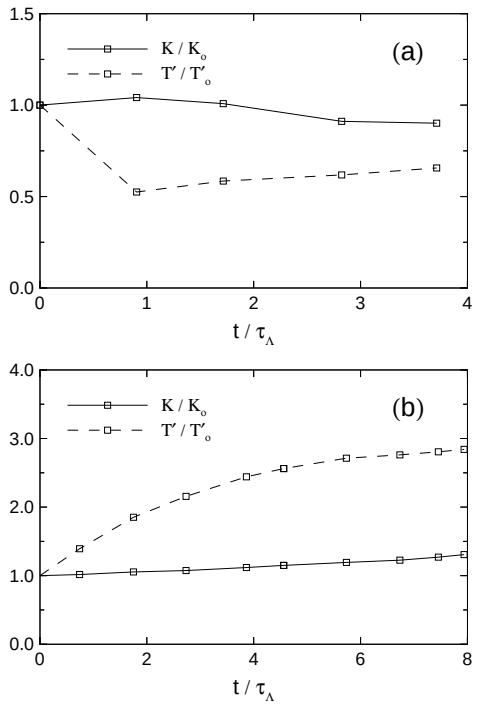

FIGURE 20. Time history of the bulk turbulent kinetic energy, $K/K_\circ$, and root-mean-squared of the temperature fluctuations, $T'/T'_\circ$, for the (a) adiabatic; and (b) isothermal reacting boundary layer simulations.

Conclusions

In this paper, we have performed direct numerical simulations of temporally evolving boundary layers at Mach 4 and $Re_\theta = 7000$ with adiabatic and isothermal wall-temperature conditions. The energy spectra and two-point correlations indicate that the numerical simulation resolution and domain size are adequate. We find that for $T_{\text{wall}} < T_{\text{adiabatic}}$ the simulations require smaller computational domains with coarser resolution in grid units, which implies finer resolution in dimensional units. The adiabatic simulation is in agreement with the theoretical and empirical prediction of the mean velocity. In contrast, the isothermal simulation does not agree with the wall and logarithmic predictions, which is puzzling. Periodic boundary conditions are found to be adequate for the time scales considered, since the growth of the displacement thickness is not significant during the time scales that we consider.

For the turbulence-chemistry interaction at the conditions chosen, we find that the relevant non-dimensional reaction rates are Da_q and Da_τ for the adiabatic and isothermal simulations, respectively. The reacting results illustrate the difference in the turbulence-chemistry interaction in the boundary layer for endothermic and exothermic reactions. We find that in the isothermal case, there is an increase in the range of turbulent scales, increased magnitude of temperature fluctuations and turbulent kinetic energy levels, larger inclination in the turbulent structure angles, and enhanced turbulent mixing. This is a result of exothermic reactions occurring near the wall. The opposite was found for the adiabatic wall simulation, where the reactions occur at the expense of the turbulent temperature fluctuations, damping the turbulent intensity and reducing the turbulent mixing. We have obtained a preliminary physical understanding of the turbulence-chemistry interactions in a high Mach number boundary layer. Further analysis at different chemical conditions are required to quantify the importance of each mechanism.

Acknowledgments

We would like to acknowledge the support from the Air Force Office of Scientific Research Grant number No. AF/F49620-98-1-0035. This work was also sponsored by the Army High Performance Computing Research Center under the auspices of the Department of the Army, Army Research Laboratory cooperative agreement number DAAH04-95-2-0003 / contract number DAAH04-95-C-0008, the content of which does not necessarily reflect the position or the policy of the government, and no official endorsement should be inferred. A portion of the computer time was provided by the University of Minnesota Supercomputing Institute.

References

[1] Johnson, H., T., Seipp, and G.V. Candler, "Numerical study of hypersonic reacting boundary layer transition to cones," *AIAA Paper No. 97-2567*, June 1997.

[2] Martín, M.P., and G.V. Candler, "Effect of chemical reactions on decaying isotropic turbulence," *Physics of Fluids*, **10**, 1715-1724, 1998.

[3] Martín, M.P. & Candler, G.V., "Subgrid-scale model for the temperature fluctuations in reacting turbulence," *Physics of Fluids,* **11**, 2765-2771, 1999.

[4] Weirs, V.G., & G.V. Candler, "Optimization of weighted ENO schemes for DNS of compressible turbulence," *AIAA Paper No. 97-1940*, 1997.

[5] Candler, G.V., W.J. Wright, and J.D. McDonald , "Data-Parallel Lower-Upper Relaxation method for reacting flows," *AIAA Journal,* 32, 2380-2386, 1994.

[6] Olejniczak, D.J., and G.V. Candler, "A Data-Parallel LU relaxation method for DNS of compressible flows," *1st International Conference in* DNS *and* LES, Louisiana, 1997.

[7] Martín, M.P., V.G. Weirs, D.O. Olejniczak, and G.V. Candler, "DNS of Reacting Hypersonic Turbulent Boundary Layers," *AIAA Paper No. 98-2917*, 1998.

[8] Jones, W.P., & Launder, B.E., "The prediction of laminarization with a two-equation model of turbulence," *International Journal of Heat and Mass Transfer,* 15, 301-314, 1972.

[9] Morkovin, M.V., "Effects of compressibility on turbulent flows," A.J. (ed) of *Mèchanique de la Turbulence*, pp. 367-380, CNRS, 1962.

[10] Reynolds, W.C., "The potential and limitations of direct and large eddy simulations," *Lecture Notes in Physics,* **357**, 313-343, 1991.

[11] Blackburn, H.M., Mansour, N.N., and Cantwell, B.J., "Topology of fine-scale motions in turbulent channel flow," *Journal of Fluid Mechanics*, **310**, 269-292, 1996.

[12] Zhou, J., Adrian, R.J., Balachandar, S., and Kendall, T.M., "Mechanisms for generating coherent packets of hairpin vortices in channel flow," *Journal of Fluid Mechanics,* **387**, 353-396, 1999.